Bachelor Thesis – UT Confidential

Improving detection depth of DiffMag handheld probe: optimizing excitation parameters

Cathryn Bruijnis

18-9-2022

Examination Committee:
Dr. Ir. L. Alic
Prof. Dr. Ir. B. ten Haken
Prof. Dr. Ir. L. Abelmann

Magnetic Detection and Imaging Group

Faculty of Science and Technology

University of Twente

Enschede

The Netherlands

MD&I UNIVERSITY OF TWENTE. | TECHMED CENTRE

List of abbreviations

B	Magnetic field
CE	Conformitè Europëenne
CV	Coefficient of Variation
DiffMag	Differential Magnetometry
duty-cycle	Active duration of the excitation sequence
f_{AC}	AC frequency
FDA	Food and Drug Administration
I_{AC}	AC current
I_{DC}	DC current
LN	Lymph Node
SLN	Sentinel Lymph Node
SLNB	Sentinel Lymph Node Biopsy
SPAQ	Superparamagnetic Quantifier
SPION	Superparamagnetic Iron-Oxide nanoparticle
ΔU	Amplitude of signal modulation
τ-cycle	DiffMag cycle

Abstract

Het lokaliseren van schildwachtklieren door de detectie van een radioactieve tracer is bewezen effectief te zijn. Nadelen van een radioactieve tracer zijn de dosis en halveringstijd die vermeden kunnen worden door Superparamagnetische ijzer Oxide Nanodeeltjes (SPIONs) als tracer te gebruiken. De Sentimag Magnetometer® is gebaseerd op lineaire magnetische detectie wat resulteert in het detecteren van alle magnetische signalen in de omgeving van de probe. De DiffMag handheld probe (MD&I, University of Twente) vermijdt dit door alleen non-lineaire magnetisatie te meten. De detectie diepte is daarentegen nog steeds een limiterende factor en kan verbeterd worden door het optimaliseren van excitatie parameters.

In deze studie zijn de optimale excitatie parameter waarden bepaald en beoordeeld met betrekking tot de detectie diepte. Magtrace® is gebruikt als tracer. De detectie diepte was verbeterd met 2 mm met AC frequentie = 4 kHz, AC stroom = 0.7 A en DC stroom = 1 A.

Table of Contents

1. Introduction

There are various methods to avoid cancer recurrence, whereas the removal of lymph nodes (LN) one of the least negatively affecting methods to the well-being of patients. Removal of the first LNs directly draining the primary tumour, referred to as sentinel lymph nodes (SLN) is a measure to mitigate the post-operative healing. Current-standard-of care for this surgical procedure, SLN biopsy (SLNB) [1] is facilitated by a radioactive tracer injected peritoumorally that spreads from the injection spot through the lymphatic system. During surgery SLNs can be located through detection of the radioactive tracer with a gamma probe and be removed individually [2,3]. The commonly used radioactive tracer (Technetium-99m) has half-life-time of approximately 1 day and for many hospitals, the nuclear reactor is more than a day's travel removed [4]. Many patients do not have access to nuclear medicine, such that SNLB cannot be performed.

As superparamagnetic Iron-Oxide Nanoparticles (SPIONs) are non-radioactive, they form a solution to the disadvantages of a radioactive tracer. SPIONs have an iron-oxide core usually with a diameter ranging from 5 to 20 nm and a biocompatible polymer coating to prevent interaction with each other [5]. SPIONs do not have a half-life time and can be safely excreted, making them suitable as a contrast agent, a drug deliverer, or a tracer [6].

The Sentimag® Magnetometer (Endomag, UK) is developed for intraoperative detection of SPIONs. It is currently the only medical device approved for detecting SPIONs by the Food and Drug Administration, USA (FDA) and Conformitè Europëenne (CE) [7]. It is based on a linear magnetic detection principle, which results in detecting all magnetic signals in its proximity.

To merely measure the non-linear magnetization of SPIONs, a Differential Magnetometry (DiffMag) handheld probe (MD&I group, University of Twente, The Netherlands) has been developed, see Figure 1 [2][8]. No calibration is required before every measurement, resulting in a less tiresome process.

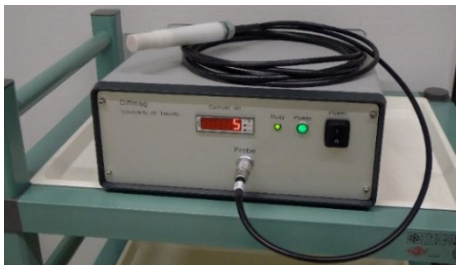

Figure 1: The DiffMag handheld probe [2].

The DiffMag handheld probe is activated by an excitation sequence which is specified by excitation parameters (see section 2.3). These parameters are defined individually and have previously been set to the following values:

- f_{AC} = 2.5 kHz
- I_{DC} = 1 A
- Duty-cycle = 40%
- I_{AC} = 0.4 A
- τ-cycle = 0.2 s

As with all handheld probes, detection depth and resolving power need to be attuned for an optimal clinical outcome. The resolving power of magnetic probes is better than radioactive probes, but the detection depth is approximately 10 times less [9]. While the detection depth of the DiffMag handheld probe is 2 mm higher than the Sentimag®, it still can be considered a limiting factor for some procedures [9]. This raises the following research question: *Which combination of the excitation parameters f_{AC}, I_{AC} and I_{DC} maximises the detection depth of the DiffMag handheld probe?*

2. Background

2.1. Magnetic behaviour

Ferromagnetic and superparamagnetic materials exhibit a non-linear magnetic behaviour under influence of a (weak) magnetic field, see Figure 2. Ferromagnetic materials consist of domains whose spins are aligned as in Figure 3a when a magnetic field is applied [10][11]. A hysteresis loop occurs as several domains must return to the original orientation. Superparamagnetism is similar to ferromagnetism, yet it only consists of one domain as the materials are so small [12]. A hysteresis loop does not occur (Figure 2) which simplifies detection by only defining the magnitude and not the direction of the magnetization [13].

Paramagnetic and diamagnetic materials create linear magnetic signals when a magnetic field is applied (Figure 2). Free particles of paramagnetic materials become weakly ionized and point in the same direction as the magnetic field (Figure 3b) [11,12]. The electrons of diamagnetic materials point in the opposite direction of the applied field, see Figure 3c. The human body and surgical instruments are considered linear magnetic materials.

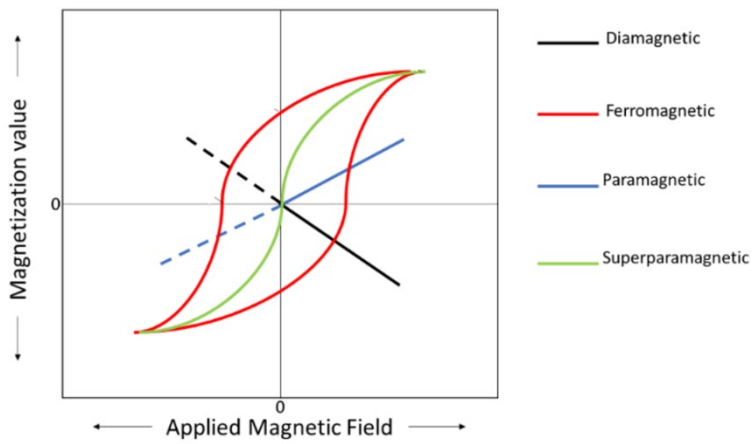

Figure 2: Relationship between magnetization value and applied magnetic field of different magnetic materials [22].

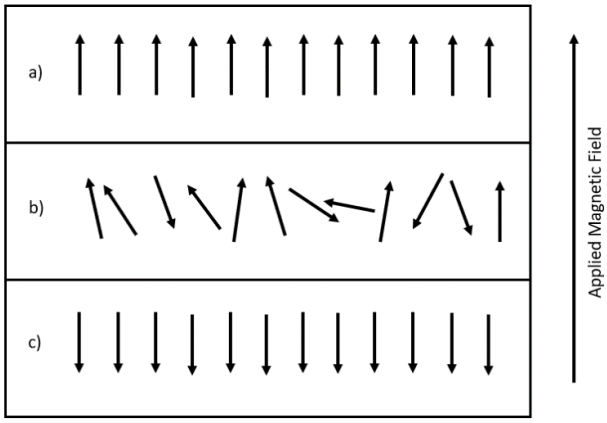

Figure 3: Magnetic field direction of a) ferro- and superparamagnetic materials, b) paramagnetic materials and c) diamagnetic materials [23].

2.2. Sentimag Magnetometer

The Sentimag® magnetometer measures both linear and non-linear magnetic signals in its proximity, leading to much noise signal. A calibration is required before every measurement to partially compensate for the noise, making the process time consuming. Although Sentimag® has its limitations, clinical studies reveal that Sentimag® is a feasible alternative to the current radioactive procedure [14] [15].

2.3. DiffMag handheld probe

The DiffMag handheld probe consists of an excitation coil and detection coil. The excitation coil is activated by PARCEVAL software version 269 (developed at MD&I, University of Twente) where an excitation sequence is defined. The excitation sequence contains of a continuous, sine-wave AC field frequency (f_{AC}) with an amplitude I_{AC}, and DC-offset fields for field excitation [16] [17]. Four values for the DC-offset fields are used per excitation sequence: DC-offset = 0 A, DC-offset = negative, DC-offset = 0 A and DC-offset = positive, see Figure 4. The absolute amplitude of the DC-offset field is called the DC current (I_{DC}), the duty-cycle is the active duration of the excitation sequence, and the DiffMag-cycle (τ-cycle) is the duration of one excitation sequence. The duration of one DC-offset value is ¼ of the τ-cycle.

The DC-offset field excites the SPIONs and the surrounding tissue. The magnetic response of the SPIONs to the AC field is then modulated while the responding signal of the tissue is not, see Figure 5. The detection coils detect this difference via Faraday's principle of induction. The amplitude of the signal modulation (ΔU) is the average difference between the resulting signal with and without a DC-offset [2] [8] [12]. The attenuation of the magnetic field (B) created by the excitation coil decreases with the third power of the distance to the source [18].

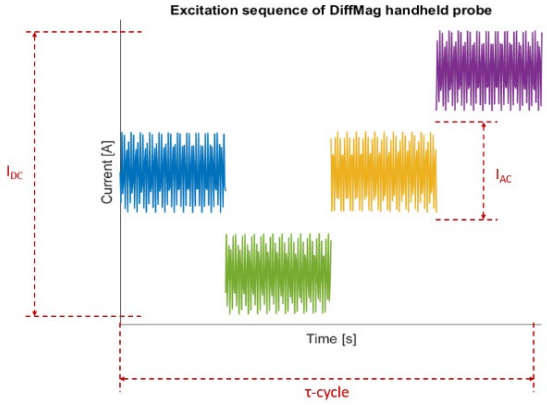

Figure 2: Excitation sequence with no DC-offset field (blue), a negative DC-offset field (green), no DC-offset field (yellow) and a positive DC-offset field (purple) [8].

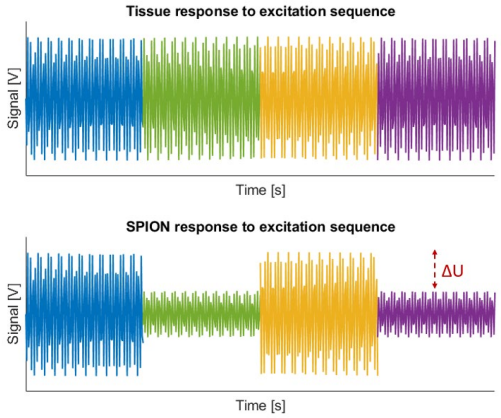

Figure 3: Resultant detector voltage of tissue without modulation (above) and SPIONs with modulation (below).

Another part of the DiffMag handheld probe is the temperature sensor [18]. The temperature sensor has been added to the probe for clinical safety reasons and a limitation has been set to 41.7 ˚C via an external resistor. A probe requirement is that the probe can measure for 15 minutes without reaching the temperature limit.

3. Material and methods

3.1. Tracer

For all measurements Magtrace® (Endomag, UK) was used as a magnetic tracer. Magtrace® is a CE- and FDA-approved magnetic tracer containing superparamagnetic carboxydextran-coated iron-oxide nanoparticles and saline [19] [20] [21]. Four samples with a volume of 150 µl, containing 500 µg iron pipetted with 132 µl of solvent: two identical samples diluted with water, and two identical samples diluted with glycerol.

3.2. Phantom

Phantom made of polyoxymethylene (MD&I, University of Twente) was used, see Figure 6. Polyoxymethylene is non-magnetic and non-reactive to the Magtrace® [9]. The phantom consists of 13 rows each containing two small holes (capacity 5 µl) and one large hole (capacity 500 µl). The small hole has a depth of 1 mm and the large hole of 8 mm.

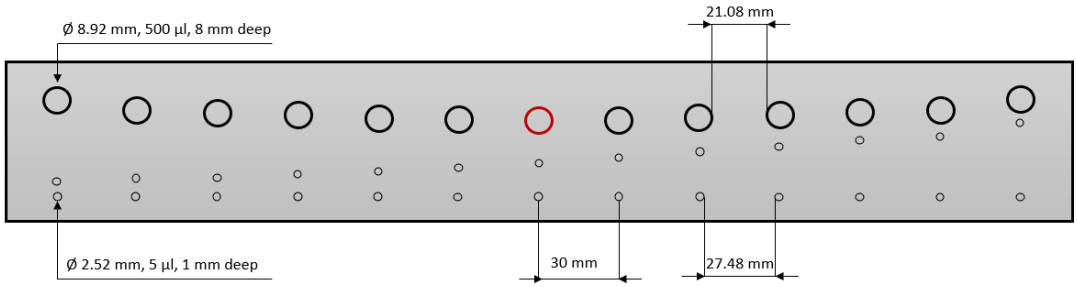

Figure 4: Open phantom with large and small holes and their dimensions. The samples are pipetted into the red hole.

3.3. Experiments

The samples were pipetted into the seventh large hole of the open phantom, shown in red in Figure 6. The DiffMag handheld probe was positioned on top of the phantom above the red hole and kept steady by using a robotic arm (Meca500, Mecademic, Canada), see Figure 7. Since 150 µl samples were used, based upon the specified phantom depth, the initial distance between the sample and the DiffMag handheld probe was 5.6 mm. All data was acquired in threefold.

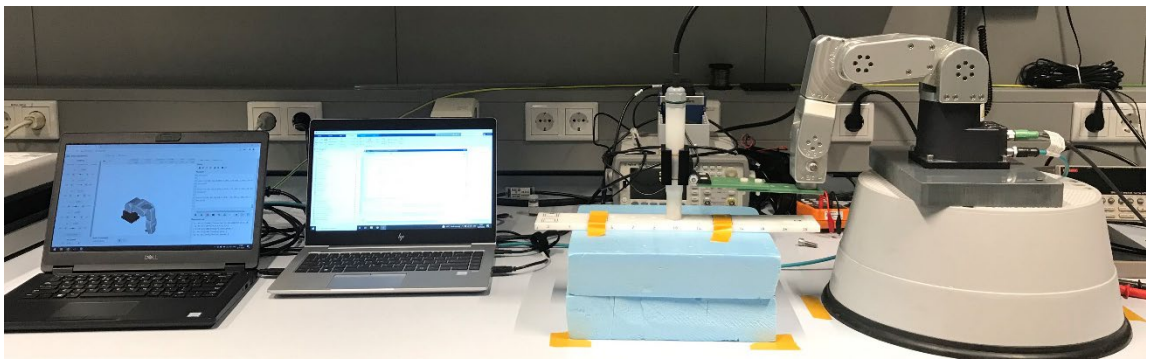

Figure 5: Experimental set-up with the robotic arm (right), the DiffMag handheld probe and open phantom (second from right) and two laptops having software for either the DiffMag handheld probe or the robotic arm.

- **Experiment I: Optimalization of excitation parameters.** For each sample, all combinations of the following excitation parameters were used to produce DiffMag detection signal:
    - f_{AC} from 1 to 11 kHz with a step size of 1 kHz
    - I_{AC} from 0.1 to 0.8 A with a step size of 0.1 A
    - I_{DC} from 0.25 to 2 A with a step size of 0.25 A.

- **Experiment II: Assessing detection depth.** The optimum combinations found in Experiment I were used to determine the detection depth. First, a background measurement was done for the combinations. Then the robotic arm moved vertically away from the phantom with a step size of 1 mm. The robotic arm pauses for 4 seconds at each interval. The measurement is stopped when the background signal was approached.

3.4. Analysis

The reproducibility is determined to assess the pipetting error. The assessment is computed by measuring under the same conditions over two separately pipetted samples (water or glycerol) and evaluated by a Bland-Altman plot. The repeatability is assessed to determine the accuracy of the DiffMag handheld probe by acquiring data in threefold for each measurement. The Coefficient of Variation (CV) of one water-diluted sample is determined and analysed.

For the Experiment 1 the DiffMag counts were averaged per dilution and the highest 1% DiffMag counts were determined with the use of the MATLAB script in Appendix I. These combinations were then used in Experiment 2 and with the MATLAB script in Appendix II, the highest detection depth was determined.

4. Results

4.1. Reproducibility and repeatability

The Bland-Altman plot to assess the pipetting error is shown in Figure 8. The data shows the proximity to the mean and is mostly situated (with a few outliers) within the limits of agreement. The CV is displayed in Figure 9 for one water-diluted sample. CV < 10% was found for 89.63% of the measurements.

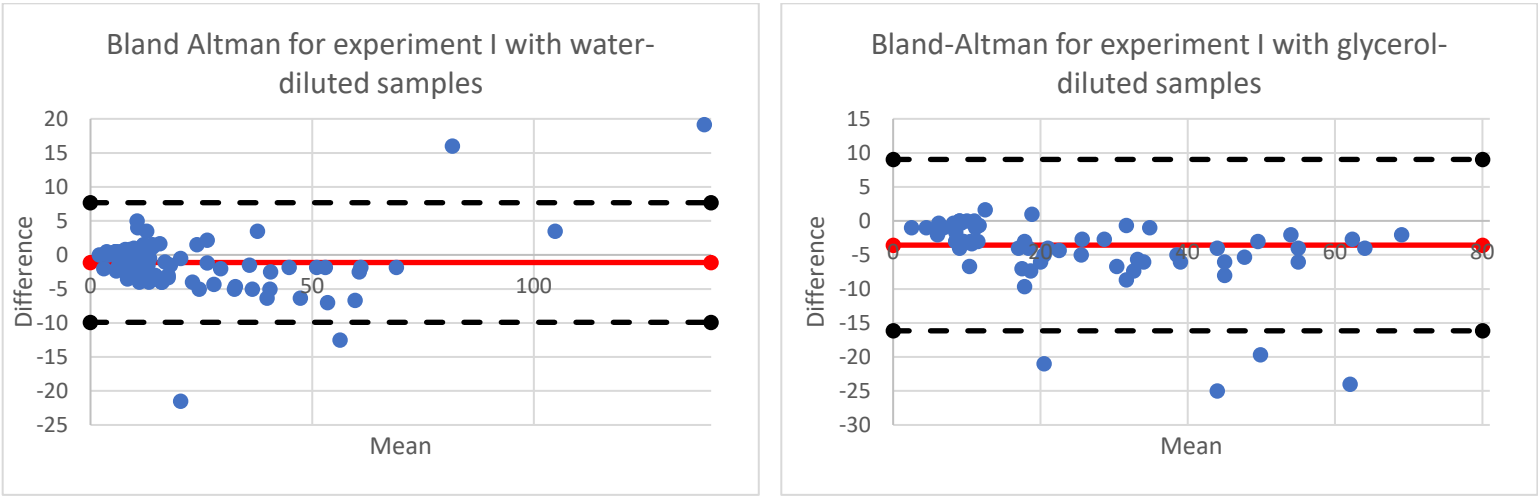

Figure 6: Bland-Altman plot for experiment I to analyse presence of pipetting error for Magtrace® diluted with water (left) and glycerol (right).

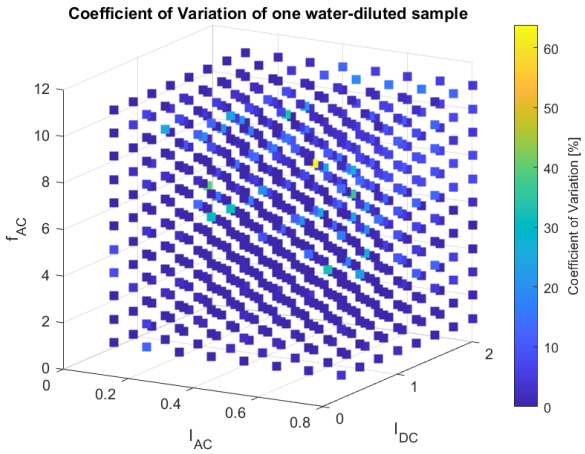

Figure 7: Coefficient of variation [%] for one water-diluted sample.

4.2. Experiment 1

Figure 10 illustrates the DiffMag counts of each excitation parameter combination for the water-diluted (left) and glycerol-diluted samples (right). The glycerol-dilutions had on average 6.9% ± 74.4% higher DiffMag counts than Magtrace® with water. For both type of samples, increasing I_{AC} and I_{DC} resulted in higher DiffMag counts. The 1% highest DiffMag counts for both sample types were determined, see Table 1.

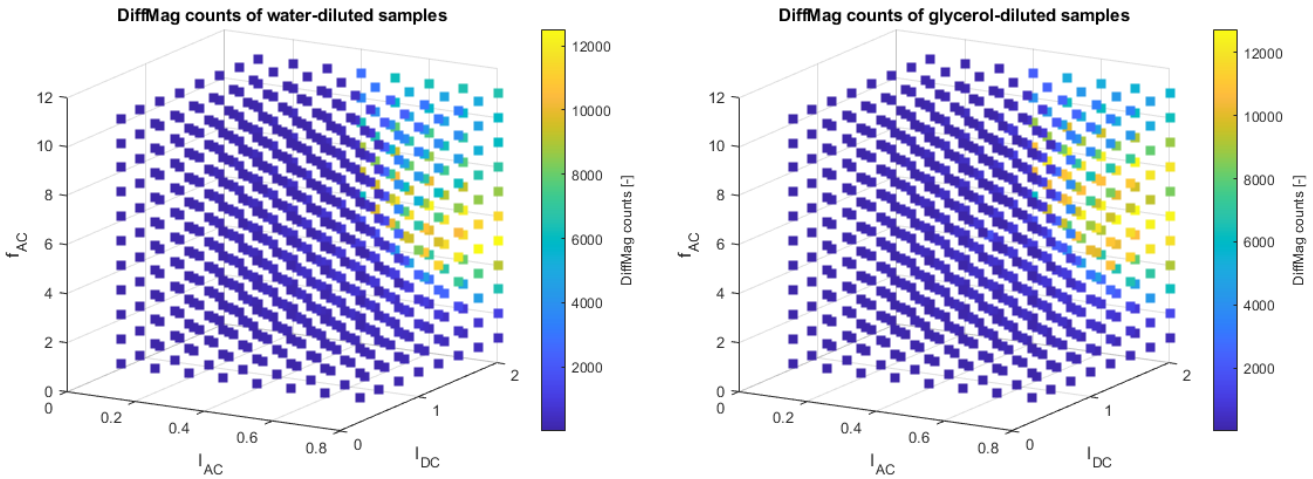

Figure 8: All excitation parameter combinations of Magtrace diluted with water (left) and glycerol (right). Higher DiffMag counts have a lighter colour.

Table 1: 1% highest DiffMag counts of water- and glycerol diluted samples with corresponding excitation parameter values.

	f_{AC} [kHz]	I_{AC} [A]	I_{DC} [A]	DiffMag counts [-]
Water	5	0.8	1.75	11482
	5	0.8	2	12515
	6	0.6	2	12246
Glycerol	6	0.7	1.75	12624
	6	0.7	2	12736
	6	0.8	2	12495
	8	0.7	2	12593

4.3. Experiment II

When using the optimum combinations from Experiment I, the temperature requirement of the DiffMag handheld probe was not met. The probe was not able to be active for 15 minutes before reaching the maximum temperature of 41.7 ˚C. Only when $I_{DC} \leq 1A$ was the DiffMag handheld probe able to fulfil the condition. The 1% highest DiffMag counts with this limitation were determined and assessed in Experiment II. An I_{AC} limitation occurred while conducting the measurements, because only a drifting signal was visible while the detection depth was increased, see Figure 11. Calibration steps did not change the resulting signal.

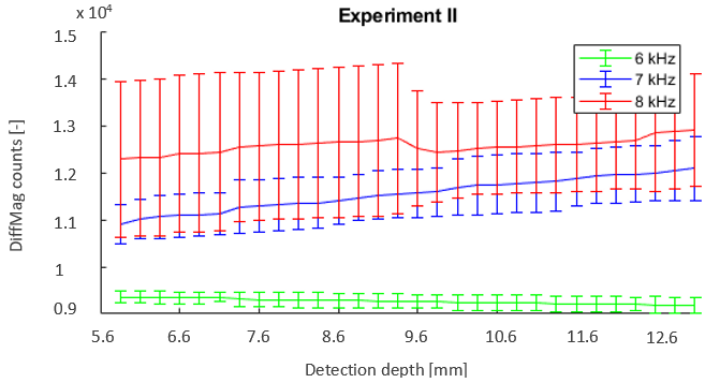

Figure 9: Detection depth results of 1% highest DiffMag counts of water samples with I_{AC} = 0.8 A, I_{DC} = 1 A, and f_{AC} = 6 kHz (green), f_{AC} = 7 kHz (blue) and f_{AC} = 8 kHz (red).

The 1% highest DiffMag counts while applying the I_{DC} and I_{AC} limitations were determined and evaluated, see Figure 12. The currently used parameter values (I_{AC} = 0.4 A, f_{AC} = 2.5 kHz, and I_{DC} = 1 A) result in a detection depth of 12.6 mm. The detection depth improved for all combinations. I_{AC} = 0.7 A, f_{AC} = 4 kHz and I_{DC} = 1 A achieved a maximum detection depth of 14.6 mm. The DiffMag counts of all measurements decreased with a third power of the distance.

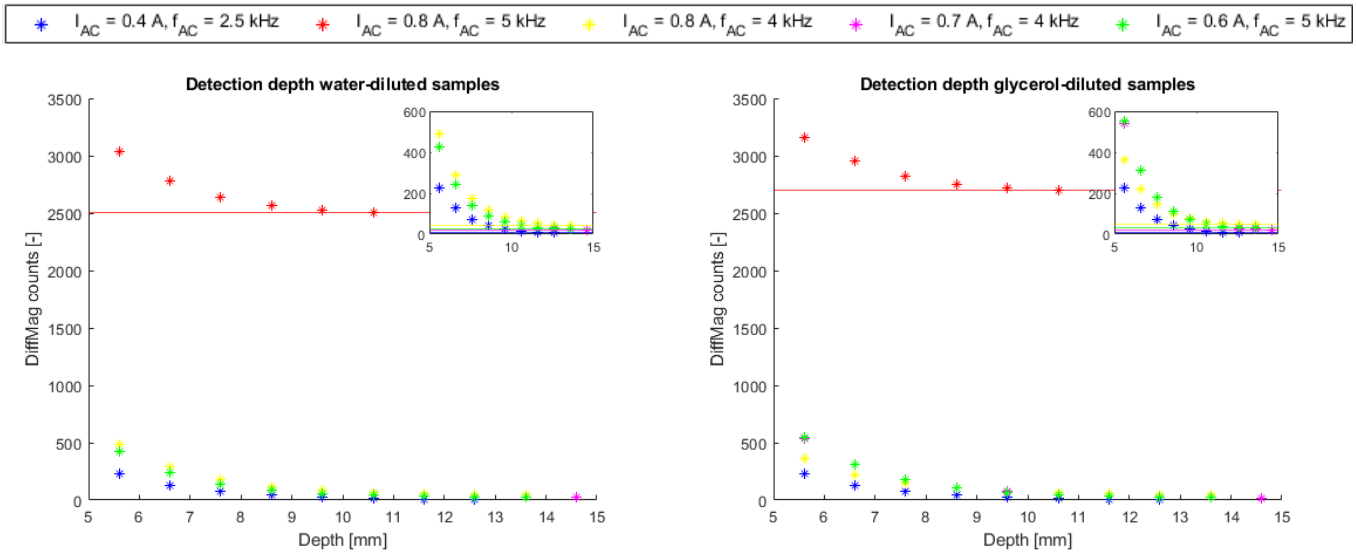

Figure 10: Detection depth for optimized excitation parameter combinations with I_{DC} = 1A for Magtrace® diluted with water (left) and glycerol (right). The horizontal lines are the background measurement for the corresponding excitation parameter combination (same colour).

5. Discussion and conclusion

A limiting detection depth is common among handheld devices. The magnetization of the SPIONs can be detected for a limited proximity, resulting in a difficulty to detect LNs deeper in the body. This study finds the optimum combination of the excitation parameters f_{AC}, I_{AC} and I_{DC} for the DiffMag handheld probe for improvement of the detection depth.

The reproducibility of the experiments was found to be adequate. A few data sets were outside the limits of agreements which were caused by a motion disturbance of the probe. The repeatability was also adequate as almost all measurements were within 10% of the mean.

I_{AC} and I_{DC} must be optimum, because the response of the SPIONs will be higher. The SPIONs are saturated by I_{DC} and the response is provoked by I_{AC}. When these parameters are too low, the saturation and response of the SPIONs will be less, resulting in a lower detection. When I_{AC} and I_{DC} are too high, the power output is too high for the hardware too handle. With a higher AC- and DC-current, a stronger magnetic field is generated and the SPIONs respond stronger, resulting in a higher ΔU. Therefore, a balance must be found such that the ΔU is as high as possible and the hardware can still manage it.

Limitations occurred in experiment II due to having a high temperature and a drifting signal. The probe could not measure for 15 minutes without reaching 42 ˚C due to a high I_{DC}. I_{DC} directly influences the probe's temperature, because more current leads to more resistance in the excitation coil and therefore in more heat energy transfer. The I_{AC} values were for all measurements below the limit (I_{DC} < 1A) hence it did not cause temperature difficulties. f_{AC} does not determine the amplitude of the signal and does not influence the probe's temperature.

The second limitation occurred for certain values of the I_{AC}. There was only a drifting signal while the detection depth was increased. A drifting signal is usually solved by a calibration, but that had no influence. Only when the I_{AC} was decreased did the drifting signal not occur.

When comparing the optimum found frequency to other studies, this found frequency is lower [12]. Since I_{AC} and I_{DC} are limited and the highest DiffMag counts in Experiment I were found at the middle of the frequency range, the optimum frequency was found at f_{AC} = 4 kHz. It is recommended to find the I_{AC} and I_{DC} limitations for $8.10 \leq f_{AC} \leq 10.96$ kHz [12] and assess the detection depth for these combinations.

The amplitude of the magnetic field (B) reduces with the third power of the distance to the origin. As said before, the SPIONs respond less when the signal is weaker resulting in lower DiffMag counts. As B decreases with a third power of the distance, so does the SPIONs response and so does the DiffMag counts, which can be seen in Figure 12. The decrease of DiffMag counts related to the distance is as expected.

The DiffMag counts of the glycerol-diluted samples were 6.9% ± 74.4% higher than the water-diluted samples. The cause of this difference is unknown and a recommendation is to compute SPAQ measurements to see how the magnetization curve differs for the dilutions.

Earlier study showed that different magnetic tracers have a different optimum f_{AC} [12], hence a recommendation is to conduct the same measurements for different magnetic tracers. Secondly, an optimization for the duty-cycle and τ-cycle with respect to the detection depth is advised. Thirdly, this paper has optimized excitation parameters for improving the detection depth, however the resolving power is also a factor that needs to be attuned. Suggested is determining the optimum combination of excitation parameters with respect to the resolving power.

To conclude, the optimum combination of excitation parameters was f_{AC} = 4 kHz, I_{AC} = 0.7 A and I_{DC} = 1 A resulting in a detection depth of 14.6 mm. An improvement of 2 mm was made with respect to the current parameter values (f_{AC} = 2.5 kHz, I_{AC} = and I_{DC} = 1 A).

6. Bibliography

[1] Amsterdam UMC. Schildwachtklierprocedure n.d. https://www.vumc.nl/zorg/expertisecentra-en-specialismen/expertisecentrum-hoofd-halstumoren/schildwachtklierprocedure.htm (accessed July 30, 2022).

[2] Waanders S, Visscher M, Wildeboer RR, Oderkerk TOB, Krooshoop HJG, Ten Haken B. A handheld SPIO-based sentinel lymph node mapping device using differential magnetometry. Phys Med Biol 2016;61:8120–34. doi:10.1088/0031-9155/61/22/8120.

[3] Loosdrecht MMV De, Molenaar L, Krooshoop EJG, Haken B Te, Meijerink WJHJ, Alic L, Broeders IAMJ. Laparoscopic Probe for Sentinel Lymph Node Harvesting Using Magnetic Nanoparticles. IEEE Trans Biomed Eng 2022;69:286–93. doi:10.1109/TBME.2021.3092437.

[4] United States Environmental Protection Agency. RAdionuclide Basics: Technetium-99 2022. https://www.epa.gov/radiation/radionuclide-basics-technetium-99 (accessed September 18, 2022).

[5] Xiao Y, Du J. Superparamagnetic nanoparticles for biomedical applications. J Mater Chem B 2020;8:354–67. doi:10.1039/c9tb01955c.

[6] Lekha GM, George S. Colloidal magnetic metal oxide nanocrystals and their applications. Elsevier Inc.; 2020. doi:10.1016/b978-0-12-813357-6.00013-9.

[7] Winter A, Engels S, Goos P, Süykers MC, Gudenkauf S, Henke RP, Wawroschek F. Accuracy of magnetometer-guided sentinel lymphadenectomy after intraprostatic injection of superparamagnetic iron oxide nanoparticles in prostate cancer: The SentiMag Pro II study. Cancers (Basel) 2020;12:1–12. doi:10.3390/cancers12010032.

[8] Visscher M, Waanders S, Krooshoop HJG, Ten Haken B. Selective detection of magnetic nanoparticles in biomedical applications using differential magnetometry. J Magn Magn Mater 2014;365:31–9. doi:10.1016/J.JMMM.2014.04.044.

[9] Mir N. Performance of handheld probes for Sentinel lymph node detection. University of Twente, 2021.

[10] Kong LB, Liu L, Yang Z, Li S, Zhang T, Wang C. Theory of ferrimagnetism and ferrimagnetic metal oxides. Elsevier Inc.; 2018. doi:10.1016/B978-0-12-811180-2.00015-3.

[11] Billah A. Investigation of multiferroic and photocatalytic properties of Li doped BiFeO3 nanoparticles prepared by ultrasonication. Diss BANGLADESH Univ Eng Technol 2017:23–35. doi:10.13140/RG.2.2.23988.76166.

[12] Hendrix MMM. To optimize the detection of magnetic nanoparticles. University of Twente, 2021.

[13] Bertotti G. Magnetic Hysteresis. Hysteresis Magn 1998:3–30. doi:10.1016/B978-012093270-2/50050-7.

[14] Douek M, Klaase J, Monypenny I, Kothari A, Zechmeister K, Brown D, Wyld L, Drew P, Garmo H, Agbaje O, Pankhurst Q, Anninga B, Grootendorst M, Ten Haken B, Hall-Craggs MA, Purushotham A, Pinder S. Sentinel node biopsy using a magnetic tracer versus standard technique: The SentiMAG multicentre trial. Ann Surg Oncol 2014;21:1237–45. doi:10.1245/s10434-013-3379-6.

[15] Karakatsanis A, Christiansen PM, Fischer L, Hedin C, Pistioli L, Sund M, Rasmussen NR, Jørnsgård H, Tegnelius D, Eriksson S, Daskalakis K, Wärnberg F, Markopoulos CJ, Bergkvist L. The Nordic SentiMag trial: a comparison of super paramagnetic iron oxide (SPIO) nanoparticles versus Tc99 and patent blue in the detection of sentinel node (SN) in patients with breast cancer and a meta-analysis of earlier studies. Breast Cancer Res Treat 2016;157:281–94. doi:10.1007/s10549-016-3809-9.

[16] Winters R. Noise in the DiffMag system. Univ Twente 2018:2–7.

[17] Van De Loosdrecht MM, Abelmann L, Ten Haken B. Experimental comparison of four nonlinear magnetic detection methods and considerations on clinical usability. Biomed Phys Eng Express 2020;7. doi:10.1088/2057-1976/abce90.

[18] Krooshoop HJG, Alic L. Probe Design 2021.

[19] Azargoshasb S, Molenaar L, Rosiello G, Buckle T, van Willigen DM, van de Loosdrecht MM, Welling MM, Alic L, van Leeuwen FWB, Winter A, van Oosterom MN. Advancing intraoperative magnetic tracing using 3D freehand magnetic particle imaging. Int J Comput Assist Radiol Surg 2022;17:211–8. doi:10.1007/s11548-021-02458-2.

[20] Endomagnetics Ltd. Instructions for use Magtrace 2018. https://www.accessdata.fda.gov/cdrh_docs/pdf16/P160053D.pdf.

[21] Endomagnetics Ltd. Magtrace ® for use with Sentimag ® 2018.

[22] Scepka T. Noninvasive control of magnetic state in ferromagnetic nanodots by Hall probe magnetometry 2016:14.

[23] Nelson N, Port J, Pandey M. Use of Superparamagnetic Iron Oxide Nanoparticles (SPIONs) via Multiple Imaging Modalities and Modifications to Reduce Cytotoxicity: An Educational Review. J Nanotheranostics 2020;1:105–35. doi:10.3390/jnt1010008.

Appendix I: MATLAB script for experiment I

```
close all; clc
% Load data manually
x1 = [0.1 0.1 0.1 0.1 0.1 0.1 0.1 0.1 0.1 0.1 0.1];
x2 = [0.2 0.2 0.2 0.2 0.2 0.2 0.2 0.2 0.2 0.2 0.2];
x3 = [0.3 0.3 0.3 0.3 0.3 0.3 0.3 0.3 0.3 0.3 0.3];
x4 = [0.4 0.4 0.4 0.4 0.4 0.4 0.4 0.4 0.4 0.4 0.4];
x5 = [0.5 0.5 0.5 0.5 0.5 0.5 0.5 0.5 0.5 0.5 0.5];
x6 = [0.6 0.6 0.6 0.6 0.6 0.6 0.6 0.6 0.6 0.6 0.6];
x7 = [0.7 0.7 0.7 0.7 0.7 0.7 0.7 0.7 0.7 0.7 0.7];
x8 = [0.8 0.8 0.8 0.8 0.8 0.8 0.8 0.8 0.8 0.8 0.8];
y1 = [0.25 0.25 0.25 0.25 0.25 0.25 0.25 0.25 0.25 0.25
0.25];
y2 = [0.5 0.5 0.5 0.5 0.5 0.5 0.5 0.5 0.5 0.5 0.5];
y3 = [0.75 0.75 0.75 0.75 0.75 0.75 0.75 0.75 0.75 0.75
0.75];
y4 = [1 1 1 1 1 1 1 1 1 1 1];
y5 = [1.25 1.25 1.25 1.25 1.25 1.25 1.25 1.25 1.25 1.25
1.25];
y6 = [1.5 1.5 1.5 1.5 1.5 1.5 1.5 1.5 1.5 1.5 1.5];
y7 = [1.75 1.75 1.75 1.75 1.75 1.75 1.75 1.75 1.75 1.75
1.75];
y8 = [2 2 2 2 2 2 2 2 2 2 2];
z = 1:1:11;

for i = 1:1:8
   for k = 1:1:11
      input_1(i,k) = data.average_all(i,1,k);
   end
   for k = 1:1:11
      input_2(i,k) = data.average_all(i,2,k);
   end
   for k = 1:1:11
      input_3(i,k) = data.average_all(i,3,k);
   end
   for k = 1:1:11
      input_4(i,k) = data.average_all(i,4,k);
   end
   for k = 1:1:11
      input_5(i,k) = data.average_all(i,5,k);
   end
   for k = 1:1:11
      input_6(i,k) = data.average_all(i,6,k);
   end
   for k = 1:1:11
      input_7(i,k) = data.average_all(i,7,k);
   end
   for k = 1:1:11
      input_8(i,k) = data.average_all(i,8,k);
   end
end

figure(2)
hold all
scatter3(x1,y1,z,70,input_1(1,:),'filled', 's')
scatter3(x2,y1,z,70,input_1(2,:),'filled', 's')
scatter3(x3,y1,z,70,input_1(3,:),'filled', 's')
scatter3(x4,y1,z,70,input_1(4,:),'filled', 's')
scatter3(x5,y1,z,70,input_1(5,:),'filled', 's')
scatter3(x6,y1,z,70,input_1(6,:),'filled', 's')
scatter3(x7,y1,z,70,input_1(7,:),'filled', 's')
scatter3(x8,y1,z,70,input_1(8,:),'filled', 's')

scatter3(x1,y2,z,70,input_2(1,:),'filled', 's')
scatter3(x2,y2,z,70,input_2(2,:),'filled', 's')
scatter3(x3,y2,z,70,input_2(3,:),'filled', 's')
scatter3(x4,y2,z,70,input_2(4,:),'filled', 's')
scatter3(x5,y2,z,70,input_2(5,:),'filled', 's')
scatter3(x6,y2,z,70,input_2(6,:),'filled', 's')
scatter3(x7,y2,z,70,input_2(7,:),'filled', 's')
scatter3(x8,y2,z,70,input_2(8,:),'filled', 's')

scatter3(x1,y3,z,70,input_3(1,:),'filled', 's')
scatter3(x2,y3,z,70,input_3(2,:),'filled', 's')
scatter3(x3,y3,z,70,input_3(3,:),'filled', 's')
scatter3(x4,y3,z,70,input_3(4,:),'filled', 's')
scatter3(x5,y3,z,70,input_3(5,:),'filled', 's')
scatter3(x6,y3,z,70,input_3(6,:),'filled', 's')
scatter3(x7,y3,z,70,input_3(7,:),'filled', 's')
scatter3(x8,y3,z,70,input_3(8,:),'filled', 's')

scatter3(x1,y4,z,70,input_4(1,:),'filled', 's')
scatter3(x2,y4,z,70,input_4(2,:),'filled', 's')
scatter3(x3,y4,z,70,input_4(3,:),'filled', 's')
scatter3(x4,y4,z,70,input_4(4,:),'filled', 's')
scatter3(x5,y4,z,70,input_4(5,:),'filled', 's')
scatter3(x6,y4,z,70,input_4(6,:),'filled', 's')
scatter3(x7,y4,z,70,input_4(7,:),'filled', 's')
scatter3(x8,y4,z,70,input_4(8,:),'filled', 's')

scatter3(x1,y5,z,70,input_5(1,:),'filled', 's')
scatter3(x2,y5,z,70,input_5(2,:),'filled', 's')
scatter3(x3,y5,z,70,input_5(3,:),'filled', 's')
scatter3(x4,y5,z,70,input_5(4,:),'filled', 's')
scatter3(x5,y5,z,70,input_5(5,:),'filled', 's')
scatter3(x6,y5,z,70,input_5(6,:),'filled', 's')
scatter3(x7,y5,z,70,input_5(7,:),'filled', 's')
scatter3(x8,y5,z,70,input_5(8,:),'filled', 's')

scatter3(x1,y6,z,70,input_6(1,:),'filled', 's')
scatter3(x2,y6,z,70,input_6(2,:),'filled', 's')
scatter3(x3,y6,z,70,input_6(3,:),'filled', 's')
scatter3(x4,y6,z,70,input_6(4,:),'filled', 's')
scatter3(x5,y6,z,70,input_6(5,:),'filled', 's')
scatter3(x6,y6,z,70,input_6(6,:),'filled', 's')
scatter3(x7,y6,z,70,input_6(7,:),'filled', 's')
scatter3(x8,y6,z,70,input_6(8,:),'filled', 's')

scatter3(x1,y7,z,70,input_7(1,:),'filled', 's')
scatter3(x2,y7,z,70,input_7(2,:),'filled', 's')
scatter3(x3,y7,z,70,input_7(3,:),'filled', 's')
scatter3(x4,y7,z,70,input_7(4,:),'filled', 's')
scatter3(x5,y7,z,70,input_7(5,:),'filled', 's')
scatter3(x6,y7,z,70,input_7(6,:),'filled', 's')
scatter3(x7,y7,z,70,input_7(7,:),'filled', 's')
scatter3(x8,y7,z,70,input_7(8,:),'filled', 's')

scatter3(x1,y8,z,70,input_8(1,:),'filled', 's')
scatter3(x2,y8,z,70,input_8(2,:),'filled', 's')
scatter3(x3,y8,z,70,input_8(3,:),'filled', 's')
scatter3(x4,y8,z,70,input_8(4,:),'filled', 's')
scatter3(x5,y8,z,70,input_8(5,:),'filled', 's')
scatter3(x6,y8,z,70,input_8(6,:),'filled', 's')
```

```
scatter3(x7,y8,z,70,input_8(7,:),'filled', 's')
scatter3(x8,y8,z,70,input_8(8,:),'filled', 's')

view(30,15)
xlabel('I_{AC}'), ylabel('I_{DC}'), zlabel('f_{AC}')
title('DiffMag counts of water-diluted samples')
grid on
cb = colorbar;
cb.Label.String = 'DiffMag counts [-]';
```

Appendix II: MATLAB script for experiment II

```
close all;clc
% load experiment_II.xlsx as numeric
matrix
data = experimentII;
avg = data(85:94,1:20);

depth = avg(:,1);

figure(1)
hold on
scatter(depth,avg(:,2),'*','Mark-
erEdgeColor','b');
scatter(depth,avg(:,3),'*','Mark-
erEdgeColor','r')
scatter(depth,avg(:,4),'*','Mark-
erEdgeColor','y')
scatter(depth,avg(:,6),'*','Mark-
erEdgeColor','m')
scatter(depth,avg(:,5),'*','Mark-
erEdgeColor','g')
xlim([5 15])
xlabel('Depth [mm]'), ylabel('DiffMag
counts [-]')
title('Detection depth water-diluted
samples')
yline(2509,'r')
hold off

ax1 = axes('Position',[0.65 0.65 0.25
0.25],'Box','on');
hold on
scatter(ax1,depth,avg(:,2),'*','Mark-
erEdgeColor','b')
scatter(ax1,depth,avg(:,4),'*','Mark-
erEdgeColor','y')
scatter(ax1,depth,avg(:,6),'*','Mark-
erEdgeColor','m')
scatter(ax1,depth,avg(:,5),'*','Mark-
erEdgeColor','g')
yline(6,'b')
yline(42,'y')
yline(21,'m')
yline(26,'g')
hold off


%%
figure(2)
hold on
scatter(depth,avg(:,16),'*','Mark-
erEdgeColor','b')
scatter(depth,avg(:,17),'*','Mark-
erEdgeColor','r')
scatter(depth,avg(:,18),'*','Mark-
erEdgeColor','y')
scatter(depth,avg(:,20),'*','Mark-
erEdgeColor','m')
scatter(depth,avg(:,19),'*','Mark-
erEdgeColor','g')
xlim([5 15])
xlabel('Depth [mm]'), ylabel('DiffMag
counts [-]')
title('Detection depth glycerol-di-
luted samples')
yline(2704,'r')
hold off

ax2 = axes('Position',[0.65 0.65 0.25
0.25],'Box','on');
hold on
scatter(ax2,depth,avg(:,16),'*','Mark-
erEdgeColor','b')
scatter(ax2,depth,avg(:,18),'*','Mark-
erEdgeColor','y')
scatter(ax2,depth,avg(:,20),'*','Mark-
erEdgeColor','m')
scatter(ax2,depth,avg(:,19),'*','Mark-
erEdgeColor','g')
yline(6,'b')
yline(48,'y')
yline(21,'m')
yline(30,'g')
hold off
```